5-10-2007

Joint Hα and X-ray observations of massive X-ray binaries. III. The Be X-ray binaries HDE 245770 = A0535+26 and X persei

E. D. Grundstrom
Georgia State University

T. S. Boyajian
Georgia State University

C. Finch
Georgia State University

D. R. Gies
Georgia State University

W. Huang
Georgia State University

See next page for additional authors

Recommended Citation

Grundstrom, E., Boyajian, T., Finch, C., Gies, D., Huang, W., Mcswain, M., O'Brien, D., Riddle, R., Trippe, M., Williams, S., Wingert, D., & Zaballa, R. (2007). Joint Hα and X-ray observations of massive X-ray binaries. III. The Be X-ray binaries HDE 245770 = A0535+26 and X persei. *Astrophysical Journal, 660* (2 I), 1398-1408. https://doi.org/10.1086/514325

Joint Hα and X-Ray Observations of Massive X-Ray Binaries. III. The Be X-ray Binaries HDE 245770 = A 0535+26 and X Persei

E. D. Grundstrom[1], T. S. Boyajian[1], C. Finch, D. R. Gies[1], W. Huang[1,2], M. V. McSwain[1,3,4], D. P. O'Brien, R. L. Riddle[1,5], M. L. Trippe, S. J. Williams[1], D. W. Wingert[1], and R. A. Zaballa

Center for High Angular Resolution Astronomy and Department of Physics and Astronomy, Georgia State University, P. O. Box 4106, Atlanta, GA 30302-4106;

erika@chara.gsu.edu, tabetha@chara.gsu.edu, finch@chara.gsu.edu, gies@chara.gsu.edu, wenjin@astro.caltech.edu, mcswain@astro.yale.edu, obrien@chara.gsu.edu, riddle@tmt.org, trippe@chara.gsu.edu, swilliams@chara.gsu.edu, wingert@chara.gsu.edu, rzaballa1@student.gsu.edu

ABSTRACT

We present results from an Hα monitoring campaign of the Be X-ray binary systems HDE 245770 = A 0535+26 and X Per. We use the Hα equivalent widths together with adopted values of the Be star effective temperature, disk inclination, and disk outer boundary to determine the half-maximum emission radius of the disk as a function of time. The observations of HDE 245770 document the rapid spectral variability that apparently accompanied the regeneration of a new circumstellar disk. This disk grew rapidly during the years 1998 – 2000, but then slowed in growth in subsequent years. The outer disk radius is probably truncated by resonances between the disk gas and neutron star orbital periods. Two recent X-ray outbursts appear to coincide with the largest disk half-maximum emission radius attained over the last decade. Our observations of X Per indicate that its circumstellar disk has recently grown to near record proportions, and concurrently the system has dramatically increased in X-ray flux, presumably the result of enhanced mass accretion from the disk. We find that the Hα half-maximum emission radius of the disk surrounding X Per reached a size about six times larger than the stellar radius, a value, however, that is well below the minimum separation between the Be star and neutron star. We suggest that spiral arms excited by tidal interaction at periastron may help lift disk gas out to radii where accretion by the neutron star companion becomes more effective.

Subject headings: stars: emission-line, Be — stars: individual (A 0535+26, HD 245770, X Per) — stars: neutron — X-rays: binaries

1. Introduction

Be X-ray binaries (BeXRBs) consist of rapidly rotating B-stars with neutron star companions (Coe 2000). The B-star primaries lose mass into an outflowing circumstellar disk, and if the disk reaches a radius comparable to the periastron separation, then disk gas accreted by the neutron star can power a significant (and often transient) X-ray source (Okazaki & Negueruela 2001; Okazaki et al. 2002). The disk gas is de-

[1]Visiting Astronomer, Kitt Peak National Observatory, National Optical Astronomy Observatory, operated by the Association of Universities for Research in Astronomy, Inc., under contract with the National Science Foundation.

[2]Current address: Department of Astronomy, California Institute of Technology, MC 105-24, Pasadena, CA 91125

[3]Current Address: Astronomy Department, Yale University, New Haven, CT 06520-8101

[4]NSF Astronomy and Astrophysics Postdoctoral Fellow

[5]Current Address: Thirty Meter Telescope, 2632 E. Washington Blvd., Pasadena, CA 91107

tected through observations of emission lines, an optical/infrared excess, and a net linear polarization caused by starlight scattered in the disk (Porter & Rivinius 2003). Be star disks are inherently time variable and can develop and disappear on timescales of years to decades (Underhill & Doazan 1982; Hubert & Floquet 1998). Thus, we expect that the X-ray accretion fluxes will vary on similar timescales. Here we present a joint study of the disk Hα emission flux and X-ray flux variations in two of the best studied BeXRBs, HDE 245770 = A 0535+26 and X Persei. We discuss similar covariations of Hα emission and X-ray flux in companion papers on the black hole binary Cyg X-1 = HDE 226868 (Gies et al. 2003), the supergiant binary LS I +65 010 (Grundstrom et al. 2007a), and the BeXRB microquasar LS I +61 303 (Grundstrom et al. 2007b).

The remarkable Be star HDE 245770 (and X-ray counterpart A 0535+26) is one of the prototype objects of the BeXRB class. The primary star of HDE 245770 has a classification of O9.7 IIIe (Giovannelli & Sabau Graziati 1992) or B0 IIIe (Steele et al. 1998), but the luminosity class is still somewhat controversial since many of the luminosity criteria are based on spectral lines that are affected by disk emission (Wang & Gies 1998). The orbital period from peaks in the X-ray flux is approximately 110 d (Hutchings 1984; Coe et al. 2006), and a comparison of the times of maxima between the first and most recent epochs suggests a period of $P = 109.96 \pm 0.05$ d. The only reliable estimate of the other orbital elements comes from X-ray timing of the pulsar spin period during three outbursts in 1993 (Finger et al. 1994; Bildsten et al. 1997), and this solution indicates that the orbital eccentricity is $e = 0.47 \pm 0.02$. The radial velocity curve of the Be star has an amplitude that is smaller than or comparable to the velocity fluctuations introduced by emission contamination and other factors, so only upper limits are available for the Be star's semiamplitude and the system mass ratio, $M_2/M_1 < 0.12$ (Wang & Gies 1998). The star has a long and rich history of X-ray, optical, and infrared observations (Motch et al. 1991; Giovannelli & Sabau Graziati 1992; Clark et al. 1998; Negueruela et al. 1998; Haigh, Coe, & Fabregat 2004; Coe et al. 2006). Lyuty & Zaitseva (2000) present a remarkable record of the light curve variations back to the year 1898, and they show that after a quiescent stage in the first part of the century the star brightened by some 40% in the early 1970s. The circumstellar disk that appeared then provided the gas to power the X-ray source at the time coincident with the dawn of X-ray astronomy.

The emission from the disk of HDE 245770 in the form of optical and infrared continuum light and Balmer emission lines displays large temporal variations in the record since the 1970s (Clark et al. 1998; Lyuty & Zaitseva 2000; Haigh et al. 2004). The dominant timescales of variability are $\sim$ 1500 d and 103 d, where the latter is the beat period of the long and orbital periods (Haigh et al. 2004). Haigh et al. (2004) argue that the disk IR flux tends to hover around three different brightness levels, and they suggest that these correspond to distinct disk radii that are defined by resonances between the disk gas and neutron star orbital periods. Okazaki & Negueruela (2001) developed a model to predict the resonant disk truncation radii in BeXRBs, and Haigh et al. (2004) found that the model predictions are consistent with the IR magnitude jumps. Coe et al. (2006) extended this analysis with additional JHK photometry and measurements of the Hα emission line. The Hα emission variations (Clark et al. 1998; Haigh et al. 1999; Lyuty & Zaitseva 2000; Haigh et al. 2004; Coe et al. 2006) indicate that the disk almost totally disappeared in 1998 but rebounded to its former strength over the next few years.

The binary system X Per (HD24534; B0 Ve, Lyubimkov et al. 1997) is the brightest and perhaps most famous member of the BeXRB class. X Per has displayed time variable optical emission lines since the earliest photographic spectrograms were made at the beginning of the last century (Cowley et al. 1972). The long term changes in the spectral appearance are reviewed by Roche et al. (1993) and Clark et al. (2001). In a seminal paper, Clark et al. (2001) describe the photometric and spectroscopic variations observed over the period 1987 through 2001, and during this time the star made a remarkable transformation from Be to B and back again to Be. Clark et al. (2001) discuss how these variations are related to the structural properties of the circumstellar disk. The orbital elements were deter-

mined by Delgado-Martí et al. (2001) by careful timing observations of the X-ray pulsar (pulse period $\approx$ 835 s) using the *Rossi X-Ray Timing Explorer (RXTE)* satellite. The orbital period is $P = 250.3$ d and the orbital eccentricity is $e = 0.11$.

Both HDE 245770 and X Per are among some hundred objects regularly observed with the *RXTE* All-Sky Monitor (ASM) instrument (Levine et al. 1996), and here we address the issue of how their disk size variations are related to the observed X-ray fluxes. We present our recent observations of their Hα emission lines in §2. We then show in §3 how the Hα emission strength is related to the disk radius, and we use these relations in §4 to document how the disk radius variations relate to the V-band and X-ray light curves. The disk radii appear to attain limits that are probably related to resonant truncation radii (Okazaki & Negueruela 2001), and we discuss in §5 how such limits affect the mass transfer process in these binaries. An appendix to the paper offers a reassessment of the orbital motion of X Per based upon radial velocity measurements of UV spectra from the *International Ultraviolet Explorer (IUE)* satellite, from which we derive limits on the binary's mass ratio and inclination.

2. Observations and Hα Variations

We observed both HDE 245770 and X Per between 1998 August and 2000 December with the Kitt Peak National Observatory 0.9 m coudé feed telescope. We used two spectrograph arrangements to record the red spectral region around Hα with resolving powers of $R = \lambda/\triangle\lambda = 4100$ and 9500. The details about the spectra and their reduction for these runs are given in a companion paper (Grundstrom et al. 2007a). In addition to these primary runs, we obtained several more spectra during auxiliary runs in 2004 October and 2006 October (using grating B in second order for a resolving power $R = 9500$ over the range 6470 – 7140 Å and 6433 – 7143 Å, respectively). All the spectra record the Hα emission line and the He I λ6678 feature.

The general trends in the spectra are illustrated in Figures 1 – 3. We show in Figure 1 the set of spectra of HDE 245770 from the 1998 August – September run that coincided with the time of disk loss. The spectra are arranged with their continua set at the time of observation and scaled so that 1 d along the y-axis corresponds to 10% of the continuum flux. We also show a model spectrum at the bottom of the figure that is derived from the grid of non-local thermodynamic equilibrium and line-blanketed model atmospheres calculated by Lanz & Hubeny (2003). This synthetic spectrum is based on the parameters of effective temperature $T_{\rm eff} = 28000$ K, gravity $\log g = 3.3$, and solar abundances (Giovannelli & Sabau Graziati 1992). The spectrum was broadened by a simple convolution with a rotational broadening function using a linear limb darkening coefficient of 0.24 (Wade & Rucinski 1985) and a projected rotational velocity of $V \sin i = 230$ km s^{-1} (Giovannelli & Sabau Graziati 1992; Wang & Gies 1998; Haigh et al. 2004). We see that there is evidence of residual emission components in both the Hα and He I λ6678 absorption lines at this time. The profiles also display significant night-to-night or faster variations. For example, there are well defined structures within the core of He I λ6678 that may result from photospheric nonradial pulsations (see the case of the similar star ζ Oph; Kambe et al. 1997), and there are variations in the relative strengths of the violet and red emission peaks in Hα. These suggest that mass loss processes leading to the development of the new disk were already underway at this time. Note that the model indicates that a line blend should be present for the C II λ6578, 6582 doublet, which appears to be absent from the HDE 245770 spectra. These lines weaken at higher temperature, but an increase in temperature would result in a model He I λ6678 profile weaker than observed. The absence of the C II features (and the weakness of the C IV profiles in the UV; Wang & Gies 1998) may point to a carbon deficiency caused by the presence of CNO-processed gas in the atmosphere of HDE 245770.

The disk emission strength of HDE 245770 had increased dramatically by the time of the next runs in 1999. We show in Figure 2 the average spectrum from each of the runs with the continuum levels offset for clarity. The growth in the Hα emission is accompanied by the appearance of emission in He I λ6678 that almost totally obscures the profile during the runs in 2000. Note how the separation between the violet and red peaks of Hα decreases

as the emission strengthens.

We show in Figure 3 the average spectrum of X Per from each of the runs, and we see that Hα and He I λ6678 were emission lines during this time. The overall morphology and strength of the lines agree well with the more extended time series presented by Clark et al. (2001). Inspection of Figure 7 in Clark et al. (2001) shows that our observations were made while the disk was active and generally increasing in strength.

We made a number of measurements to characterize the profile variations of Hα for both stars, and these are summarized in Table 1 (given in full in the electronic version). Column 1 lists the target name, column 2 gives the heliocentric Julian date of mid-exposure, and column 3 shows the corresponding orbital phase (from the ephemeris of Finger et al. 1994 for HDE 245770 and from Delgado-Martí et al. 2001 for X Per). Column 4 lists the equivalent width determined by a numerical integration of the line flux over the range 6536 – 6590 Å. We measured the radial velocity of the wings based upon a bisector position determined using the method of Shafter, Szkody, & Thorstensen (1986). This method samples the line wings using oppositely signed Gaussian functions and determines the mid-point position between the wings by cross-correlating these Gaussians with the profile. We used Gaussian functions with FWHM = 200 (100) km s^{-1} at sample positions in the wings of $\pm$320 ($\pm$190) km s^{-1} for HDE 245770 (X Per), and these radial velocities are given in column 5 of Table 1. Zamanov et al. (1999) advocated making fits of double-peaked Hα profiles using Gaussian functions to match the violet V and red R peaks, and we have followed their approach here, although we caution that such a functional fit is poor in many instances. These double-Gaussian fits were restricted to the inner part of the profile ($|\triangle\lambda| < 6$ Å for HDE 245770 and $< 2-4$ Å for X Per) since the wings are much more extended that those of Gaussian functions. The remaining columns in Table 1 list the parameters for these fits: radial velocity of the V peak (col. 6), radial velocity of the R peak (col. 7), ratio of the equivalent widths of the V and R components (col. 8), V/R peak intensity ratio (col. 9), FWHM for the V peak (col. 10), and FWHM for the R peak (col. 11). Note that Hα has only one peak in the 2006 observations of X Per, so we fit a single Gaussian to the profiles of these three spectra.

We find no compelling evidence that these fitting parameters vary with orbital phase, although we caution that our orbital phase coverage is incomplete. In particular, the radial velocity measurements for the Hα wings and emission peaks do not appear follow the orbital motion expected for the Be star (see Wang & Gies 1998 for HDE 245770 and the Appendix for X Per). We suspect that these velocity measurements are dominated by fluctuations related to the azimuthal distribution and non-Keplerian motion of the disk gas, and these variations confound attempts to measure the much smaller orbital motion in our data sets. The best strategy for measuring the orbital radial velocities of these Be stars may be to wait until an episode of disk loss occurs and then embark on a program of high dispersion, high S/N spectroscopy of emission-free lines in the blue part of the spectrum.

3. Disk Radius and Hα Strength

The Hα emission forms primarily in the disk surrounding the Be star, and the total flux of the feature (measured as the line equivalent width) is closely related to the size of the disk. In a recent paper (Grundstrom & Gies 2006) we present calculations of the disk size and emission strength for an extensive range of stellar and disk properties. The Be disk models are based upon a simple parameterization of disk properties outlined by Hummel & Vrancken (2000), from which we derive a synthetic Hα line profile and the angular distribution on the sky of the wavelength integrated Hα flux. The model predictions about the emission strength and angular size of the disks agree with observational results for bright Be stars whose disks have been resolved through optical long baseline interferometry.

The disk model assumes an axisymmetric gas structure with the gas density distribution set by a power law R^{-m} (where R is the distance from the rotational axis), an exponential decline above and below the disk, and a base density at the star's surface. The disk surface brightness is set by its temperature, and we assume an isothermal disk with a gas temperature of $0.6T_{\rm eff}$ where $T_{\rm eff}$ is the effective temperature of the Be star. The spatial

flux distribution is integrated along segments normal to the major axis of the projected disk to obtain a collapsed emission sum as a function of position along the major axis. We adopted a working definition of disk radius as the distance along the major axis from the star where the integrated Hα emission intensity of the disk declines to half of the peak value found at a position immediately adjacent to the photosphere (the half-width at half-maximum intensity radius or HWHM radius for short).

The functional relationship between Hα equivalent width and disk HWHM radius for a specific Be star depends upon the star's $T_{\rm eff}$, the inclination of the disk normal to the line of sight, and the adopted outer boundary for the disk radius (Grundstrom & Gies 2006). We list in Table 2 the values of these parameters that we adopt for HDE 245770 and X Per. The listed radii and masses are estimates from Okazaki & Negueruela (2001) and Lyubimkov et al. (1997) and the stellar effective temperatures are from Giovannelli & Sabau Graziati (1992) and Lyubimkov et al. (1997) for HDE 245770 and X Per, respectively. We assume that the disk is co-planar with the orbit, and we adopt the mid-range estimates of inclination from Wang & Gies (1998) and the Appendix for HDE 245770 and X Per, respectively. We set the outer boundary for the model disk equal to the Be star's Roche radius at apastron. The results are generally insensitive to this last assumption, since the Hα flux is small from the outer, optically thin portions of the disk. The predicted relationships between equivalent width W_λ[Hα] and the ratio of the disk HWHM radius to the stellar radius R_d/R_s are shown in Figure 4 for a large range in disk base density. The model equivalent width is referenced to the photospheric flux, and if the disk contributes a continuum flux fraction of $\epsilon = F_\lambda^d/F_\lambda^s$ then the observed equivalent width must be prorated by a factor of $(1+\epsilon)$ in order to find the ratio of the disk to star radius R_d/R_s from Figure 4.

There are several features of these simple models that need to be considered in the derivation of a disk HWHM radius from the Hα equivalent width. First, if the disk temperature differs from our assumed value of $0.6T_{\rm eff}$, then the predicted Hα equivalent width will change by a factor of approximately $T_{\rm disk}/(0.6T_{\rm eff})$ for a given disk radius. This is due to the fact the disk gas source function varies almost linearly with temperature for Hα in hot Be stars like these two targets. Second, the equatorial gas density is assumed to follow a power law R^{-m} with $m = 3.0$, the value often derived in studies of the IR flux excess of Be stars. The numerical relationship between W_λ[Hα] and R_d/R_s is relatively insensitive to the selected value of m (Grundstrom & Gies 2006), although the base density for any position along the curve depends critically on m. We caution, however, that the actual disk density properties may vary significantly from a power law in these BeXRBs. For example, if the star experiences an episode of increased disk mass loss, a density enhancement may appear to propagate outwards over time and produce increased emission strength when the enhancement reaches the radius of the optically thick/thin boundary. Using the disk radius derived from the relation in Figure 4, we would correctly determine that the HWHM radius had increased but we would err if we assumed that the emission strengthening results from an increase in density at all radii.

Finally, it is possible the disk may be truncated by tidal or resonant effects at a radius smaller than our assumed outer boundary. If the disk density drops to zero in the outer optically thin zone, then only a small part of the total emission is lost and we would only slightly overestimate the emission flux for a given HWHM radius. Thus, the revised curves would appear slightly above those shown in Figure 4 (see an example of the variation with outer boundary in Fig. 1 of Grundstrom & Gies 2006) and our derived HWHM radii will be slightly smaller than the actual values. On the other hand, if the disk density vanishes at a radius where the gas is optically thick, then the revised curves will reach an asymptotic limit slightly below the cut-off radius. The resulting functions would fall below the standard curves at the high emission end in Figure 4, and we would then tend to overestimate the HWHM radii using the standard relations. The former case probably applies to the two targets we analyze here, since the HWHM radii we find are generally small compared to the suspected truncation radii (we discuss this further in §4). Thus, the HWHM radii measurements we derive may slightly underestimate the actual values. Our analysis is insufficient to detect the presence of a truncation radius, but if one exists, its radius

will be larger than the HWHM radius.

4. Disk Growth and X-ray Accretion Flux

The mass transfer rate and subsequent accretion-driven X-ray flux will clearly depend on the changes in the radius of the Be star's disk that we can track through the variations in the Hα equivalent widths. Here we consider the long term variations in the Be star's disk as observed in the Hα emission flux and in the disk continuum flux (as seen in the observed V-band light curve). We then compare the derived disk radius variations with those observed in the X-ray light curves from the *RTXE*/ASM instrument (Levine et al. 1996).

4.1. HDE 245770

Lyuty & Zaitseva (2000) note that the V-band continuum of HDE 245770 may be much brighter than the stellar continuum alone (due to continuum light from the disk), and consequently the observed equivalent width referred to the combined continuum flux may underestimate the absolute Hα emission flux. In order to compare the Hα emission flux to a constant stellar continuum, we need to rescale the equivalent width by the factor $1+\epsilon$ where ϵ gives the ratio of the monochromatic disk-to-stellar continuum flux at wavelengths near Hα. Following Lyuty & Zaitseva (2000), we can estimate the rescaled flux by comparing the V magnitude at the time of the Hα measurement with the magnitude of the star alone, $V = 9.50$, by

$$(1+\epsilon)\ W_\lambda = 10^{-0.4(V-9.50)}\ W_\lambda. \qquad (1)$$

Lyuty & Zaitseva (2000) present V magnitudes for dates contemporaneous with the Hα measurements through 1998, and we have used these to make the small corrections from equation (1). However, there are no published estimates of V for the succeeding years, so instead we relied on surrogate measurements of the J magnitude from Coe et al. (2006) in order to make these corrections. Haigh et al. (2004) (see their Fig. 1) show how the infrared magnitude variations track those observed in the V-band for HDE 245770, and we used a series of photometric V (Lyuty & Zaitseva 2000) and J observations (Coe et al. 2006) over a common time span to find a relation between these for HDE 245770,

$$(V - 9.50) = 0.32(J - 8.67), \qquad (2)$$

which has an empirical scatter of ± 0.03 mag. We used the observed J magnitudes from Coe et al. (2006) with equation (2) to find V and transform the equivalent widths from 1999 onwards to an absolute scale. We then used Figure 4 to find estimates of the disk HWHM emission radius for the times of the Hα observations.

The observed light curve and derived disk HWHM radii are plotted in the middle and lower panels of Figure 5. The disk HWHM radii are derived from our W_λ data together with like measurements from Giovannelli et al. (1999), Lyuty & Zaitseva (2000), Piccioni et al. (2000a), Haigh et al. (2004), and Coe et al. (2006). We see that the disk almost disappeared in 1998 and then started to grow rapidly in radius over the next two years. The expansion rate slowed considerably by 2001 at a radius of $R_d/R_S \approx 4$. However, subsequent observations show that the disk continued to grow slowly and reached a maximum radius of $R_d/R_S \approx 5$ by 2005.

Coe et al. (2006) also present a time evolution diagram of disk radius (see their Fig. 7) that they derive from the velocity separation $\triangle V$ of the violet and red peaks of the Hα profile (Huang 1972). Their method leads to somewhat smaller radii than our HWHM radii ($\approx 83\%$ as large using $\triangle V$ measurements derived from Table 1) because the radius derived from $\triangle V$ is based upon a velocity sampling weighted by the brighter parts of the disk while the HWHM radius corresponds to an outer boundary between the bright and faint parts of the disk. The two depictions of disk evolution are in general agreement except for estimates from 2005 August where Coe et al. determine a disk radius about twice as large as indicated in our Figure 5. We think this discrepancy is due to the fact Coe et al. relied on an extrapolation of a linear relationship between W_λ[Hα] and $\triangle V$ to estimate radius for the 2005 August data (for which no direct $\triangle V$ measurements were available). If one adopts a standard power law relation between these variables (Zamanov et al. 2001) rather than a linear fit (which tends to underestimate $\triangle V$ for strong emission), then the extrapolation leads to radii similar to those shown in Figure 5 for 2005 August.

We also show in the lower panel of Figure 5 dotted lines that indicate disk HWHM radii derived from mean levels of Hα strength in the

past that were highlighted in the review by Lyuty & Zaitseva (2000) (and indicated in their Fig. 3). The lower two levels correspond to the two groupings of Hα strength observed between 1987 and 1998 while the upper level shows the much larger disk HWHM radius associated with data from 1975 through 1981 when the Hα emission was exceptionally strong ($W_\lambda \approx -26$ Å, de Loore et al. 1984; $V \approx 8.9$, Lyuty & Zaitseva 2000). Note that the deceleration in disk growth observed in 2001 occurred at the time when the disk HWHM radius had reached the lower cluster level.

Haigh et al. (2004) and Coe et al. (2006) argue that the tendency for the disk emission fluxes to cluster at specified levels is related to the presence of resonances between the disk gas and neutron star orbital periods that tend to truncate the disk at specific disk radii (Okazaki & Negueruela 2001). These truncation radii are given by

$$\frac{R_n}{R_s} = \left(\frac{GM_s}{4\pi^2}\right)^{1/3} \frac{1}{R_s} \left(\frac{P_{\rm orbit}}{n}\right)^{2/3} = \frac{r(M_s/M_\odot)^{1/3}}{n^{2/3} R_s/R_\odot} \quad (3)$$

where n is the integer number of gas rotation periods per neutron star orbit and r is a constant equal to 97 if the resonance occurs with the orbital period or 92 if the resonance is with the shorter beat period (103 d; Larionov, Lyuty, & Zaitseva 2001) presumably caused by retrograde precession of the disk (Haigh et al. 2004). Okazaki & Negueruela (2001) predict that the important truncation radii for HDE 245770 will be those associated with the $n = 4$ and 5 resonances, and using their adopted parameters (Table 2) the resonance radii will occur at $R_d/R_s = 6.6$ and 5.7 for $n = 4$ and 5, respectively (for $r = 92$). The $n = 5$ truncation radius is indicated as a dashed line in the lower panel of Figure 5, and we see that the disk HWHM radius hovered slightly below this limit between 2001 and 2006. This suggests that the rapid disk growth phase ended when the outer parts of the disk reached the $n = 4$ or 5 resonance truncation radius.

The top panel of Figure 5 shows the mean X-ray fluxes[6] binned in time slots equal to one orbital period, and error bars indicate the standard deviation of the mean within the time bin. The slow expansion of the disk apparently led to the large X-ray outburst observed near JD 2,453,526 (Coe et al. 2006) and a second smaller outburst near JD 2,453,616. These outbursts occurred when the disk had reached its largest HWHM radius over the duration of the *RXTE*/ASM mission. The binary semimajor axis is approximately $17.9R_s$ (Table 2) and the periastron separation is $9.5R_s$ (shown as the *dot-dashed line* in lower panel of Fig. 5). The mean Roche radius of the Be star will be approximately $5.7R_s$ at periastron, about the size of disk HWHM radius at the time of the outbursts. This suggests that the disk had grown to a size sufficient to permit active mass transfer at periastron around the epoch when the outbursts were observed. Furthermore, the huge emission strengths observed during 1976 – 1981 indicate that the disk may have attained a HWHM radius of $R_d/R_s = 9$ then (*top dotted line* in the lower panel of Fig. 5), exceeding the Roche limit at periastron.

We suspect that the mass transfer process is probably aided by the strong tidal forces that exist near periastron. Okazaki et al. (2002) present hydrodynamical simulations for BeXRBs that show how the periastron tides excite a two-arm spiral structure in the Be star disk, and the arm closest to the neutron star can lift material far beyond the nominal disk boundary to provide a source of gas accretion at phases beyond periastron. We show in Figure 6 the X-ray light curves binned in orbital phase according to the ephemeris of Finger et al. (1994) for the three energy bands observed by *RXTE*/ASM. The time sample is restricted to quiescent (non-outburst) dates. We see that the high energy flux attains a maximum near orbital phase 0.3, i.e., well past periastron at phase 0.0. A similar phase delay in the emission strength of Hβ was detected by Motch et al. (1991). These observations suggest that the disk does become more extended for a period following periastron, leading to a delayed peak in mass transfer and X-ray emission.

4.2. X Persei

The Hα emission equivalent widths of X Per observed in 2000 and 2004 and especially in 2006 are the largest measured over the last few decades (Roche et al. 1993; Piccioni et al. 2000b; Clark et al. 2001), and they indicate that the disk

[6]http://xte.mit.edu

has grown significantly in size. Once again we need to rescale the equivalent widths to a constant stellar continuum flux level by considering the $(1+\epsilon)$ factor. We estimated this flux excess using the V-band light curve and the relation

$$(1+\epsilon)\ W_\lambda = 10^{-0.4(V-6.78)}\ W_\lambda \qquad (4)$$

where the base level magnitude of the star alone, $V = 6.78$, is that observed during the last disk-free phase (Lyubimkov et al. 1997). The V-band light curve comes from observations by the members of the American Association of Variable Star Observers (AAVSO) that we transformed to standard Johnson V magnitude using contemporaneous photometry from Zamanov & Zamanova (1995), Engin & Yuce (1997), and photoelectric measurements from the AAVSO (Percy & Bakos 2001). The transformed AAVSO measurements were binned into 25 d means to increase the S/N ratio.

Our results are plotted as function of time in Figure 7. The lower panel shows the time evolution of the disk HWHM radius derived from our Hα equivalent width measurements and other published values (Clark et al. 2001; Liu & Hang 2001; Zamanov et al. 2001). The middle panel shows the time binned V-band light curve from the AAVSO observations. We see that X Per reached a maximum of $V \approx 6.2$ in 2000 and then rose again to $V \approx 6.1$ where it has remained to the present. The circumstellar disk of X Per is now brighter than it has been for the past few decades (Roche et al. 1993). The top panel shows the binned X-ray fluxes observed with *RXTE*/ASM. We see that the first brightening episode corresponded to the onset of a slow increase in X-ray flux that eventually soared to a record high over the ASM observation period shortly after the second visual brightening. The X-ray flux continues to remain high during the current optically bright state.

The apparent increase in X-ray flux (and implied gas accretion rate) that accompanied the disk expansion confirms that the X-ray source is powered by gas from the Be star disk. However, the largest disk HWHM radius shown in Figure 7 is still much smaller than the separation between the Be star and neutron star. For example, the mean Roche radius at periastron is $34R_S$ (Table 2), which is a factor of five larger than the maximum disk HWHM radius ($R_d/R_s = 6.4$ in Fig. 7). The maximum predicted disk size due to the action of the tidally-driven eccentric instability occurs at the 3 : 1 resonance radius between the disk gas and neutron star orbital periods (Okazaki & Negueruela 2001; Clark et al. 2001), and this radius occurs at $R_d/R_s = 31$ (Table 2). Once again the observed maximum HWHM radius is smaller than the predicted truncation limit.

However, tidal forces at periastron may excite a two-armed spiral in the disk, and the spiral arm facing the companion can lift disk gas out to close to the vicinity of the neutron star (Okazaki et al. 2002). If so, mass transfer will occur predominantly after periastron as the gas in the arm extension is accreted by the neutron star. We show in Figure 8 the X-ray light curves for X Per from fluxes recorded in the recent active state (HJD > 2,452,200) that are binned according to the orbital ephemeris of Delgado-Martí et al. (2001). We see that there is an orbital modulation (particularly in the high energy band) that was not obvious in the earlier, low state data (Wen et al. 2006) and that the X-ray maximum occurs about one quarter of a period after periastron. This phase of maximum is consistent with post-periastron accretion from extended disk gas in a spiral arm.

5. Discussion

The Hα observations presented here and elsewhere document the remarkable and continuing changes that occur in the mass loss from the Be stars in these two BeXRB systems. The gas that enters their circumstellar disks becomes a reservoir of fuel for accretion by the neutron star companion, and the X-ray activity that accompanies the mass transfer increases dramatically as the disk radius increases in size. The disk growth is expected to be limited by gravitational interactions with the neutron star (Okazaki & Negueruela 2001; Okazaki et al. 2002). In low eccentricity binaries like X Per, the limiting radius occurs at the 3:1 resonance radius by the tidally-driven eccentric instability, while in high eccentricity systems like HDE 245770, the neutron star will approach closer to the Be star at periastron and higher integer resonances occurring at smaller radii will act to truncate the disk.

Our observations appear to confirm these ex-

pectations in the case of HDE 245770. The largest disk HWHM radius we find from the Hα equivalent width is comparable to both the $n = 5$ resonance radius and the mean Roche radius at the time of periastron. The historical maxima of Hα strength may imply that the disk HWHM radius can occasionally grow to even larger dimensions. We caution, however, that it may be possible for Be disks of extreme density to attain very large Hα emission fluxes without radial growth. For example, pressure broadening in high density disks can lead to an increased flux in the wings of Hα and thus a larger emission equivalent width. Whether such high density and high pressure disks could remain confined by gravitational forces is an open question.

The case of X Per, on the other hand, shows that the mass transfer and X-ray accretion flux can increase even when the disk HWHM radius attains a size well below the critical value. We found that the recent X-ray flux increase occurred when the disk HWHM radius grew to about $R_d/R_s = 5$, much less than the resonant truncation radius of $R_3/R_s = 31$. There are two probable explanations for this difference. First, tidal forces at periastron promote the development of a two-arm spiral structure in the disk (Okazaki et al. 2002) and gas concentrated in the arm closest to the companion can be pushed outwards and accreted by the neutron star. Hydrodynamical models suggest that the gas accretion rate from the spiral arm will peak sometime after periastron, and we find that indeed the X-ray flux maximum lags periastron by $\approx 25\%$ of the orbital period in both the BeXRBs examined here and in the microquasar LS I +61 303 (Grundstrom et al. 2007b). Secondly, the disk probably extends beyond the HWHM radius of the Hα emission that we use to define disk radius (Grundstrom & Gies 2006). The disk density is described in our model in terms of a power law with radial distance from the star (Hummel & Vrancken 2000), and the lower gas density at larger radius may be entirely adequate to power the accretion-driven X-ray flux.

The observational record for both of these BeXRBs documents the growth of the disk from inside out. A comparison of the V-band light curves and Hα radii in both Figures 5 and 7 shows that the time evolution of the Hα emission lags behind that of the disk continuum flux. Clark et al. (2001) also noted this delay between the line and continuum fluxes, and they argue that the time lag is due to differences in spatial origin. The continuum flux excess is probably formed in the inner part of the disk while the Hα emission is more optically thick and forms over a wider range of disk radius. Thus, an outwards propagating density enhancement would peak first in continuum light and later in the Hα flux. The fate of this outflow is unclear. Models by Okazaki et al. (2002) suggest that some of the mass falls back onto the Be star, some is accreted by the neutron star, and the remainder escapes from the system (presumably into a circumbinary region centered on the orbital plane). A search for such circumstellar structures might yield evidence of the ejected gas (for example, as a compact H II region surrounding X Per; Reynolds et al. 2005).

We thank Daryl Willmarth and the staff of KPNO for their assistance in making these observations possible. We acknowledge with thanks the variable star observations from the AAVSO International Database contributed by observers worldwide and used in this research. The X-ray results were provided by the ASM/RXTE teams at MIT and at the RXTE SOF and GOF at NASA's GSFC. The *IUE* data presented in this paper were obtained from the Multimission Archive at the Space Telescope Science Institute (MAST). STScI is operated by the Association of Universities for Research in Astronomy, Inc., under NASA contract NAS5-26555. Support for MAST for non-HST data is provided by the NASA Office of Space Science via grant NAG5-7584 and by other grants and contracts. This work was supported by the National Science Foundation under grants AST-0205297, AST-0506573, and AST-0606861. Institutional support has been provided from the GSU College of Arts and Sciences and from the Research Program Enhancement fund of the Board of Regents of the University System of Georgia, administered through the GSU Office of the Vice President for Research.

A. Mass Ratio Limit from *IUE* Radial Velocities of X Per

Several investigators have attempted to measure the orbital motion of X Per, but their results have generally been inconclusive because the lines are broad, shallow, and often marred by emission and because the semiamplitude is probably small (Hutchings 1977; Reynolds et al. 1992; Stickland 1992). The ideal spectral range to search for orbital motion is in the ultraviolet because the disk flux contribution is relatively small in the UV (Telting et al. 1998). Stickland (1992) used the spectra available at that time in the archive of the *IUE* to measure radial velocities, and he found that the velocity excursions were too small to measure orbital motion. Here we repeat the analysis of the now larger set of *IUE* spectra using the complementary orbital elements from the pulsar orbit (Delgado-Martí et al. 2001).

We obtained 43 high dispersion, short wavelength prime camera spectra of X Per from the *IUE* database maintained at the Multimission Archive at Space Telescope[7]. These spectra were transformed to a uniform $\log\lambda$, heliocentric wavelength grid, normalized to a pseudo-continuum, and excised of the main interstellar lines, and radial velocities were measured by cross-correlation (Penny, Gies, & Bagnuolo 1999). A mean formed from the average of all the spectra was used as a spectral template, and its absolute velocity was determined to be +0.8 km s^{-1} by cross-correlation with a similar spectrum of HD 34078 (Gies & Bolton 1986). We used the apparent shifts between each cross-correlation function and the ensemble mean of the functions to estimate the relative velocity shift for each spectrum, and then the final absolute velocities were set by adding the template velocity above. The results are listed in Table 3 (given in full in the electronic version) that gives the heliocentric Julian date of mid-exposure, the orbital phase from the ephemeris of Delgado-Martí et al. (2001), and the measured radial velocity.

We then fit the *IUE* velocities using the non-linear, least-squares, orbital elements program of Morbey & Brosterhus (1974). This was a constrained solution in which all the elements were set from the pulsar results (Delgado-Martí et al. 2001) (with the longitude of periastron changed by 180°) with the exception of the systemic velocity γ and the semiamplitude K. The formal solution for these parameters is $\gamma = 1.0 \pm 0.9$ km s^{-1} and $K = 2.3 \pm 1.4$ km s^{-1}, and the observations and calculated radial velocity curve are illustrated in Figure 9. Clearly the amplitude of motion is small enough that this result is of marginal significance, but the velocities do place a useful upper limit on the semiamplitude. The dotted line in Figure 9 shows the fit with a semiamplitude of $K + 2\sigma = 5.0$ km s^{-1}, and this appears to be a reasonable upper limit consistent with the spread in the *IUE* velocities.

The pulsar orbital elements (Delgado-Martí et al. 2001) give a neutron star orbital semiamplitude of $K = 39.8 \pm 0.4$ km s^{-1}, so the ratio of the upper limit of the Be star semiamplitude to that for the pulsar yields an upper limit on the mass ratio, $M_2/M_1 < 0.13$. We have plotted this constraint in the mass plane diagram in Figure 10 together with lines of constant orbital inclination derived from the pulsar mass function. A lower limit on the inclination of $i > 23°$ results from assuming that the star rotates slower than the critical rate (Clark et al. 2001). Harmanec (1988) presents a summary of mass and radii data from eclipsing binary stars, and the mass range for a B0 V star is probably between $\approx 11 M_\odot$ and $17 M_\odot$. The shaded region in Figure 10 shows this probable Be star range together with the observed range in neutron star mass (van Kerkwijk, van Paradijs, & Zuiderwijk 1995). This region in the mass plane corresponds to an inclination range of $i = 28°$ to $35°$.

[7] http://archive.stsci.edu/iue/

REFERENCES

Bildsten, L., et al. 1997, ApJS, 113, 367

Clark, J. S., Tarasov, A. E., Okazaki, A. T., Roche, P., & Lyuty, V. M. 2001, A&A, 380, 615

Clark, J. S., et al. 1998, MNRAS, 294, 165

Coe, M. J. 2000, in The Be Phenomenon in Early-Type Stars, IAU Coll. 175 (ASP Conf. Vol. 214), ed. M. A. Smith, H. F. Henrichs, & J. Fabregat (San Francisco: ASP), 656

Coe, M. J., Reig, P., McBride, V. A., Galache, J. L., & Fabregat, J. 2006, MNRAS, 368, 447

Cowley, A. P., McLaughlin, D. B., Toney, J., & MacConnell, D. J. 1972, PASP, 84, 834

Delgado-Martí, H., Levine, A. M., Pfahl, E., & Rappaport, S. A. 2001, ApJ, 546, 455

de Loore, C., et al. 1984, A&A, 141, 279

Engin, S., & Yuce, K. 1997, IBVS, 4454, 1

Fabregat, J., et al. 1992, A&A, 259, 522

Finger, M. H., Cominsky, L. R., Wilson, R. B., Harmon, B. A., & Fishman, G. J. 1994, in The Evolution of X-Ray Binaries, ed. S. S. Holt & C. S. Day (New York: AIP), 459

Gies, D. R., & Bolton, C. T. 1986, ApJS, 61, 419

Gies, D. R., et al. 2003, ApJ, 583, 424

Giovannelli, F., & Sabau Graziati, L. 1992, Space Sci. Rev., 59, 1

Giovannelli, F., Sabau-Graziati, L., Bernabei, S., & Galleti, S. 1999, IAU Circ. 7293

Grundstrom, E. D., & Gies, D. R., 2006, ApJ, 651, L53

Grundstrom, E. D., et al. 2007a, ApJ, 656, 431

Grundstrom, E. D., et al. 2007b, ApJ, 656, 437

Haigh, N. J., Coe, M. J., & Fabregat, J. 2004, MNRAS, 350, 1457

Haigh, N. J., Coe, M. J., Steele, I. A., & Fabregat, J. 1999, MNRAS, 310, L21

Harmanec, P. 1988, Bull. Astr. Inst. Cz., 39, 329

Huang, S.-S. 1972, ApJ, 171, 549

Hubert, A. M., & Floquet, M. 1998, A&A, 335, 565

Hummel, W., & Vrancken, M. 2000, A&A, 359, 1075

Hutchings, J. B. 1977, MNRAS, 181, 619

Hutchings, J. B. 1984, PASP, 96, 312

Kambe, E., et al. 1997, ApJ, 481, 406

Lanz, T., & Hubeny, I. 2003, ApJS, 146, 417

Larionov, V., Lyuty, V. M., & Zaitseva, G. V. 2001, A&A, 378, 837

Levine, A. M., Bradt, H., Cui, W., Jernigan, J. G., Morgan, E. H., Remillard, R., Shirey, R. E., & Smith, D. A. 1996, ApJ, 469, L33

Liu, Q. Z., & Hang, H. R. 2001, Ap&SS, 275, 410

Lyubimkov, L. S., Rostopchin, S. I., Roche, P., & Tarasov, A. E. 1997, MNRAS, 286, 549

Lyuty, V. M., & Zaitseva, G. V. 2000, Astr. Lett., 26, 9

Morbey, C., & Brosterhus, E. B. 1974, PASP, 86, 455

Motch, C., Stella, L., Janot-Pacheco, E., & Mouchet, M. 1991, ApJ, 369, 490

Negueruela, I., Reig, P., Coe, M. J., & Fabregat, J. 1998, A&A, 336, 251

Norton, A. J., et al. 1991, MNRAS, 253, 579

Okazaki, A. T., Bate, M. R., Ogilvie, G. I., & Pringle, J. E. 2002, MNRAS, 337, 967

Okazaki, A. T., & Negueruela, I. 2001, A&A, 377, 161

Penny, L. R., Gies, D. R., & Bagnuolo, W. G., Jr. 1999, ApJ, 518, 450

Percy, J. R., & Bakos, A. G. 2001, PASP, 113, 748

Piccioni, A., Bartolini, C., Bernabei, S., Galleti, S., Guarnieri, A., & Valentini, G. 2000b, in The Be Phenomenon in Early-Type Stars, IAU Coll. 175 (ASP Conf. Vol. 214), ed. M. A. Smith, H. F. Henrichs, & J. Fabregat (San Francisco: ASP), 585

Piccioni, A., et al. 2000a, in The Be Phenomenon in Early-Type Stars, IAU Colloquium 175 (ASP Conf. Proc. 214), ed. M. A. Smith, H. F. Henrichs, & J. Fabregat (San Francisco: ASP), 569

Porter, J. M., & Rivinius, Th. 2003, PASP, 115, 1153

Reynolds, A. P., Hilditch, R. W., Bell, S. A., Pollacco, D. L., & Edwin, R. P. 1992, MNRAS, 258, 439

Reynolds, R. J., Chaudhary, V., Madsen, G. J., & Haffner, L. M. 2005, AJ, 129, 927

Roche, P., et al. 1993, A&A, 270, 122

Shafter, A. W., Szkody, P., & Thorstensen, J. R. 1986, ApJ, 308, 765

Steele, I. A., Negueruela, I., Coe, M. J., & Roche, P. 1998, MNRAS, 297, L5

Stickland, D. J. 1992, MNRAS, 257, 21P

Telting, J. H., Waters, L. B. F. M., Roche, P., Boogert, A. C. A., Clark, J. S., de Martino, D., & Persi, P. 1998, MNRAS, 296, 785

Underhill, A. B., & Doazan, V. 1982, B Stars With and Without Emission Lines, NASA SP-456 (Washington, DC: NASA)

van Kerkwijk, M. H., van Paradijs, J., & Zuiderwijk, E. J. 1995, A&A, 303, 497

Wade, R. A., & Rucinski, S. M. 1985, A&AS, 60, 471

Wang, Z. X., & Gies, D. R. 1998, PASP, 110, 1310

Wen, L., Levine, A. M., Corbet, R. H. D., & Bradt, H. V. 2006, ApJS, 163, 372

Zamanov, R. K., Martí, J., Paredes, J. M., Fabregat, J., Ribó, M., & Tarasov, A. E. 1999, A&A, 351, 543

Zamanov, R. K., Reig, P., Martí, J., Coe, M. J., Fabregat, J., Tomov, N. A., & Valchev, T. 2001, A&A, 367, 884

Zamanov, R. K., & Zamanova, V. I. 1995, IBVS, 4189, 1

This 2-column preprint was prepared with the AAS LaTeX macros v5.2.

TABLE 1

Hα MEASUREMENTS

Star Name	Date (HJD−2,400,000)	Orbital Phase	W_λ (Å)	$V_r(W)$ (km s^{-1})	$V_r(V)$ (km s^{-1})	$V_r(R)$ (km s^{-1})	$W_\lambda(V)$ / $W_\lambda(R)$	V/R	FWHM(V) (Å)	FWHM(R) (Å)
HDE 245770	51055.969	0.103	1.76	18.4	···	···	···	···	···	···
HDE 245770	51056.989	0.112	1.96	42.4	···	···	···	···	···	···
HDE 245770	51057.960	0.121	1.41	32.4	···	···	···	···	···	···
HDE 245770	51058.950	0.130	2.16	30.5	···	···	···	···	···	···
HDE 245770	51061.954	0.157	1.96	38.0	···	···	···	···	···	···
HDE 245770	51061.993	0.158	2.07	31.7	···	···	···	···	···	···
HDE 245770	51063.962	0.176	1.62	21.1	···	···	···	···	···	···
HDE 245770	51065.981	0.194	1.05	16.5	···	···	···	···	···	···
HDE 245770	51066.902	0.202	0.52	18.0	···	···	···	···	···	···
HDE 245770	51066.976	0.203	0.88	20.3	···	···	···	···	···	···
HDE 245770	51419.972	0.403	−3.11	22.5	−147.7	165.5	0.80	0.96	4.41	5.34
HDE 245770	51419.995	0.403	−3.20	23.1	−144.9	165.6	0.80	0.95	4.68	5.52
HDE 245770	51425.987	0.458	−4.31	8.6	−158.3	161.6	0.95	0.97	5.12	5.26
HDE 245770	51428.950	0.485	−4.06	12.1	−151.8	165.0	0.96	0.98	4.97	5.10
HDE 245770	51464.958	0.811	−5.32	4.5	−157.6	156.7	0.98	1.06	4.84	5.24
HDE 245770	51464.980	0.811	−5.14	4.7	−155.8	158.8	1.00	1.05	4.89	5.14
HDE 245770	51465.936	0.820	−5.17	3.1	−156.5	154.2	0.99	1.05	4.75	5.04
HDE 245770	51465.957	0.820	−5.04	2.1	−156.6	153.9	0.99	1.03	4.81	5.01
HDE 245770	51466.906	0.829	−4.80	−3.6	−157.5	149.1	1.02	1.04	4.72	4.78
HDE 245770	51466.928	0.829	−4.79	−5.9	−158.5	149.3	1.06	1.03	4.81	4.69
HDE 245770	51467.988	0.839	−4.41	−3.6	−153.5	155.5	1.06	1.05	4.87	4.85
HDE 245770	51468.952	0.847	−4.54	−4.5	−152.6	159.5	1.22	1.06	5.28	4.61
HDE 245770	51468.974	0.847	−4.73	−1.5	−152.9	155.8	1.12	1.06	5.03	4.75
HDE 245770	51469.916	0.856	−4.87	−8.1	−155.9	152.1	1.12	1.06	5.05	4.76
HDE 245770	51491.904	0.055	−5.01	6.0	−148.6	154.3	1.01	0.97	4.96	4.78
HDE 245770	51492.833	0.064	−5.20	10.0	−148.0	153.6	0.93	1.00	4.74	5.09
HDE 245770	51493.827	0.073	−5.25	12.3	−150.5	156.9	0.92	0.98	4.82	5.10
HDE 245770	51494.869	0.082	−5.57	12.8	−147.5	163.4	0.95	1.01	4.76	5.08
HDE 245770	51494.890	0.082	−5.36	10.9	−148.5	156.6	0.96	1.01	4.74	4.98
HDE 245770	51495.944	0.092	−5.28	6.7	−148.6	157.8	1.01	0.99	4.92	4.84
HDE 245770	51496.919	0.101	−5.20	12.6	−147.7	161.0	0.94	1.00	4.69	4.98
HDE 245770	51497.852	0.109	−4.66	17.8	−144.8	161.8	0.92	0.96	4.76	4.98
HDE 245770	51817.905	0.011	−8.03	12.4	−126.1	133.5	0.92	0.96	4.77	5.00
HDE 245770	51818.908	0.020	−8.36	6.2	−120.7	136.8	1.04	0.98	5.11	4.78
HDE 245770	51819.899	0.029	−8.00	8.7	−120.8	136.4	1.04	1.00	4.96	4.77
HDE 245770	51821.884	0.047	−7.66	6.6	−121.6	132.3	0.99	0.98	4.83	4.77
HDE 245770	51822.888	0.056	−7.83	4.7	−123.3	133.3	0.99	0.98	4.89	4.84
HDE 245770	51823.830	0.065	−7.86	11.9	−119.7	134.9	0.98	1.00	4.84	4.90
HDE 245770	51823.934	0.066	−8.22	5.4	−122.1	134.8	1.01	1.01	4.93	4.92
HDE 245770	51824.855	0.074	−8.19	13.4	−121.5	134.8	0.94	0.96	4.90	5.01
HDE 245770	51824.962	0.075	−7.86	8.7	−121.9	131.6	0.94	0.99	4.76	5.02
HDE 245770	51830.913	0.129	−8.81	13.2	−115.1	140.6	1.09	1.03	5.15	4.88
HDE 245770	51890.840	0.672	−7.21	6.6	−119.4	130.1	1.03	1.01	4.84	4.76
HDE 245770	51890.861	0.672	−7.03	7.3	−120.6	129.6	1.00	0.99	4.79	4.72

TABLE 1—*Continued*

Star Name	Date (HJD−2,400,000)	Orbital Phase	W_λ (Å)	$V_r(W)$ (km s^{-1})	$V_r(V)$ (km s^{-1})	$V_r(R)$ (km s^{-1})	$W_\lambda(V)$ / $W_\lambda(R)$	V/R	FWHM(V) (Å)	FWHM(R) (Å)
HDE 245770	51892.806	0.690	−6.97	6.1	−119.8	127.1	0.98	0.99	4.79	4.83
HDE 245770	51892.827	0.690	−6.99	5.4	−117.8	130.3	1.01	0.99	4.88	4.76
HDE 245770	51893.812	0.699	−7.60	6.5	−117.2	131.6	1.04	0.99	4.96	4.71
HDE 245770	51893.833	0.699	−7.55	7.2	−114.8	134.4	1.10	0.99	5.03	4.56
HDE 245770	51894.799	0.708	−7.61	5.7	−117.9	132.9	1.08	0.99	5.08	4.67
HDE 245770	51894.823	0.708	−7.65	5.4	−118.5	132.5	1.05	0.99	4.98	4.70
HDE 245770	51895.834	0.717	−7.63	7.5	−118.2	131.4	1.04	1.00	5.00	4.80
HDE 245770	51895.913	0.718	−7.53	7.4	−117.5	131.8	1.04	1.00	4.95	4.77
HDE 245770	51896.834	0.727	−7.37	7.5	−118.7	130.3	1.00	0.99	4.84	4.79
HDE 245770	51896.855	0.727	−7.46	5.7	−117.9	132.1	1.05	1.00	5.00	4.75
HDE 245770	51897.832	0.736	−7.47	9.2	−119.2	128.6	0.98	1.00	4.81	4.94
HDE 245770	51897.853	0.736	−7.57	8.9	−118.9	129.9	1.00	1.00	4.85	4.86
HDE 245770	51898.841	0.745	−7.77	8.0	−118.8	132.2	1.03	1.00	4.89	4.77
HDE 245770	51898.862	0.745	−7.78	8.2	−119.5	132.0	1.01	1.01	4.88	4.85
HDE 245770	51899.838	0.754	−7.90	8.3	−118.8	132.8	1.02	0.99	4.96	4.81
HDE 245770	51899.859	0.754	−7.86	8.5	−118.8	134.2	1.03	0.99	5.00	4.80
HDE 245770	51900.831	0.763	−7.95	6.1	−117.8	136.2	1.11	1.00	5.18	4.69
HDE 245770	51900.852	0.763	−8.00	6.3	−120.2	135.0	1.07	1.00	5.14	4.83
HDE 245770	51901.817	0.772	−7.87	8.3	−115.8	136.5	1.11	1.00	5.18	4.65
HDE 245770	51901.838	0.772	−7.79	9.4	−117.2	135.0	1.06	0.99	5.09	4.77
HDE 245770	54019.981	0.975	−10.08	0.5	−119.4	103.1	0.82	0.82	4.92	4.94
HDE 245770	54020.953	0.984	−10.21	2.8	−116.3	105.8	0.80	0.84	4.77	4.99
HDE 245770	54021.957	0.993	−10.16	3.1	−113.7	105.9	0.84	0.83	4.88	4.81
X Per	51055.896	0.811	−9.38	4.5	−73.1	93.0	0.79	0.92	2.71	3.16
X Per	51056.966	0.815	−9.09	4.6	−72.3	94.5	0.77	0.91	2.71	3.22
X Per	51057.948	0.819	−9.64	4.4	−71.2	93.5	0.82	0.92	2.74	3.09
X Per	51058.938	0.823	−9.50	4.0	−70.4	95.1	0.85	0.92	2.81	3.06
X Per	51061.986	0.835	−9.51	0.6	−67.6	92.5	0.99	0.93	2.92	2.74
X Per	51062.915	0.839	−9.49	0.8	−69.1	91.1	0.93	0.93	2.84	2.85
X Per	51063.954	0.843	−9.09	1.2	−68.9	92.5	0.90	0.90	2.85	2.85
X Per	51065.936	0.851	−9.25	0.7	−67.2	92.0	1.00	0.90	2.96	2.66
X Per	51066.937	0.855	−8.99	−1.1	−68.1	90.4	0.96	0.90	2.86	2.70
X Per	51491.878	0.553	−10.05	−15.1	−116.4	62.0	0.71	0.77	3.65	3.97
X Per	51492.818	0.557	−10.15	−11.8	−113.5	64.2	0.70	0.77	3.58	3.94
X Per	51493.813	0.561	−10.24	−10.6	−110.2	67.6	0.76	0.80	3.72	3.91
X Per	51494.845	0.565	−10.31	−12.5	−111.4	65.9	0.77	0.80	3.74	3.91
X Per	51494.853	0.565	−10.27	−12.4	−112.3	65.5	0.75	0.80	3.68	3.92
X Per	51495.873	0.569	−10.30	−11.7	−109.0	67.8	0.78	0.82	3.67	3.85
X Per	51496.859	0.573	−10.21	−13.5	−113.6	63.0	0.71	0.80	3.55	4.03
X Per	51497.830	0.577	−10.22	−12.9	−115.1	61.7	0.68	0.79	3.52	4.09
X Per	51817.899	0.855	−18.63	17.5	−42.7	118.6	2.29	2.05	3.17	2.83
X Per	51818.900	0.859	−18.69	16.0	−43.1	118.0	2.30	2.10	3.14	2.87
X Per	51819.887	0.863	−18.54	15.7	−43.0	115.8	2.34	2.09	3.13	2.79
X Per	51820.918	0.867	−18.59	15.7	−43.5	116.3	2.31	2.13	3.13	2.88

TABLE 1—*Continued*

Star Name	Date (HJD−2,400,000)	Orbital Phase	W_λ (Å)	$V_r(W)$ (km s^{-1})	$V_r(V)$ (km s^{-1})	$V_r(R)$ (km s^{-1})	$W_\lambda(V)$ / $W_\lambda(R)$	V/R	FWHM(V) (Å)	FWHM(R) (Å)
X Per	51821.873	0.871	−18.42	14.5	−43.5	116.4	2.41	2.15	3.12	2.79
X Per	51822.875	0.875	−18.49	14.7	−42.5	115.8	2.40	2.12	3.13	2.76
X Per	51823.823	0.879	−18.26	14.5	−42.3	116.1	2.47	2.15	3.15	2.74
X Per	51824.852	0.883	−18.53	15.8	−41.6	115.6	2.37	2.09	3.15	2.77
X Per	51824.959	0.884	−18.39	16.7	−40.9	116.3	2.37	2.08	3.15	2.76
X Per	51830.954	0.908	−19.59	11.9	−49.3	105.4	1.95	1.89	3.04	2.96
X Per	51888.787	0.139	−18.93	7.8	−59.0	104.3	1.75	1.85	3.09	3.26
X Per	51888.792	0.139	−18.95	8.9	−58.5	104.9	1.71	1.84	3.07	3.31
X Per	51889.738	0.142	−18.54	8.3	−59.1	99.9	1.66	1.86	3.01	3.38
X Per	51889.872	0.143	−19.32	7.5	−58.4	101.1	1.74	1.89	3.04	3.30
X Per	51890.733	0.146	−19.21	7.7	−58.4	101.0	1.73	1.91	3.02	3.34
X Per	51892.756	0.154	−18.91	5.4	−59.6	100.0	1.83	1.91	2.99	3.12
X Per	51893.769	0.158	−19.00	7.6	−59.2	102.6	1.74	1.91	2.98	3.26
X Per	51894.767	0.162	−18.76	9.1	−57.7	102.8	1.76	1.80	2.99	3.07
X Per	51895.824	0.167	−18.64	9.0	−55.2	103.7	1.84	1.81	3.06	3.01
X Per	51896.797	0.171	−19.03	8.7	−55.0	103.7	1.92	1.83	3.08	2.94
X Per	51897.797	0.175	−18.85	8.2	−55.5	104.3	1.91	1.85	3.07	2.98
X Per	51898.806	0.179	−18.97	8.4	−55.0	105.2	1.93	1.85	3.10	2.97
X Per	51899.804	0.183	−18.93	8.7	−55.3	104.1	1.91	1.84	3.07	2.96
X Per	51900.797	0.187	−18.83	8.9	−54.0	105.5	1.95	1.89	3.09	2.99
X Per	51901.783	0.191	−19.26	9.0	−52.4	107.2	2.06	1.97	3.07	2.93
X Per	53290.922	0.740	−17.71	−9.7	−80.7	53.6	0.66	0.87	2.65	3.46
X Per	53290.926	0.740	−17.61	−9.4	−80.7	56.8	0.81	0.92	2.89	3.28
X Per	53292.922	0.748	−18.12	−9.3	−78.3	56.2	0.78	0.93	2.74	3.26
X Per	53292.928	0.748	−17.93	−9.1	−82.4	51.7	0.59	0.83	2.57	3.64
X Per	54019.950	0.653	−23.81	−6.4	−8.9	···	···	···	7.92	···
X Per	54020.939	0.657	−23.61	−4.4	−6.9	···	···	···	7.78	···
X Per	54021.930	0.661	−24.38	−4.5	−7.2	···	···	···	7.78	···

Table 2

Adopted Stellar and Disk Parameters

Parameter	HDE 245770	X Per
R_s ($R_\odot$) ..	15.	6.5
M_s ($M_\odot$) .	20.	15.5
T_s (K)	28000	29500
i (deg)	28.5	31.5
$R_{\rm outer}$ (R_s)	15.9	42.9

Table 3

IUE Radial Velocity Measurements

Date (HJD−2,400,000)	Orbital Phase	V_r (km s^{-1})
43602.749	0.034	−5.3
43705.644	0.445	3.3
43712.142	0.471	20.4
43784.061	0.758	6.2
43796.362	0.808	7.5
43850.204	0.023	4.3
43885.683	0.164	5.8
43885.749	0.165	−3.5
43885.806	0.165	−5.6
43947.719	0.412	1.6
44156.035	0.245	−0.7
44231.213	0.545	3.8
44319.029	0.896	−3.2
44319.087	0.896	−5.2
44319.138	0.896	−0.3
44319.187	0.896	−4.3
44319.238	0.897	−4.3
44319.279	0.897	−9.4
44323.732	0.915	2.3
44327.924	0.931	0.7
44582.952	0.950	−0.6
44582.991	0.950	4.2
44888.132	0.169	−3.9
48118.467	0.075	−4.4
49593.258	0.967	5.8
49593.325	0.968	2.1
49621.183	0.079	−0.2
49621.275	0.079	1.1
49643.343	0.168	−4.0
49647.365	0.184	−1.0
49715.074	0.454	2.5
49715.112	0.454	10.0
49715.159	0.454	6.3
49715.198	0.455	0.2
49748.731	0.589	0.2
49748.796	0.589	−0.9
49775.778	0.697	8.2
49775.824	0.697	7.0
49956.299	0.418	2.9
50000.094	0.593	−4.1
50104.187	0.009	−15.1
50124.212	0.089	1.2
50144.055	0.168	1.0

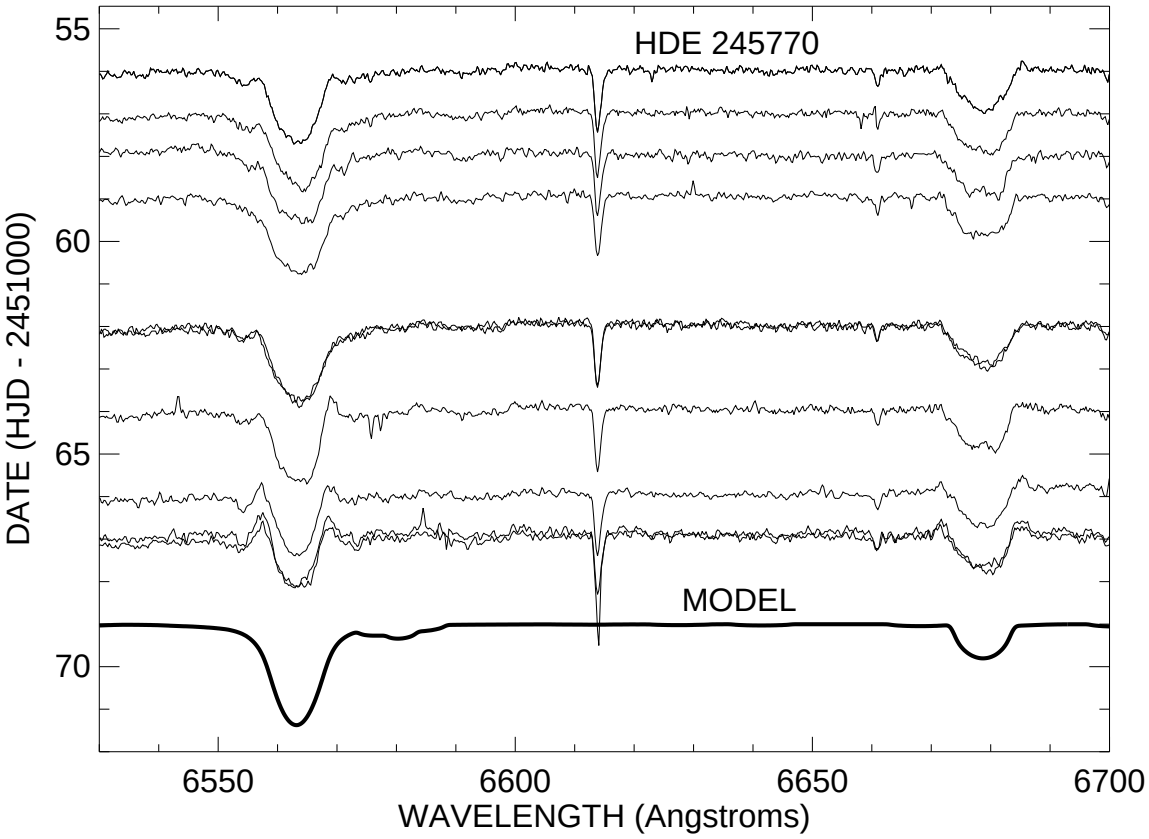

Fig. 1.— A sequence of red spectra of HDE 245770 from 1998 when the the disk had almost disappeared. Each spectrum has its continuum aligned with the heliocentric Julian date of observation, and each is scaled in flux so that 10% of the continuum equals 1 d of time. The bottom synthetic spectrum represents a model with $T_{\rm eff} = 28000$ K, $\log g = 3.3$, and $V \sin i = 230$ km s^{-1}. The features present include the stellar Hα λ6563 and He I λ6678 lines and the interstellar features at 6613 Å and 6660 Å.

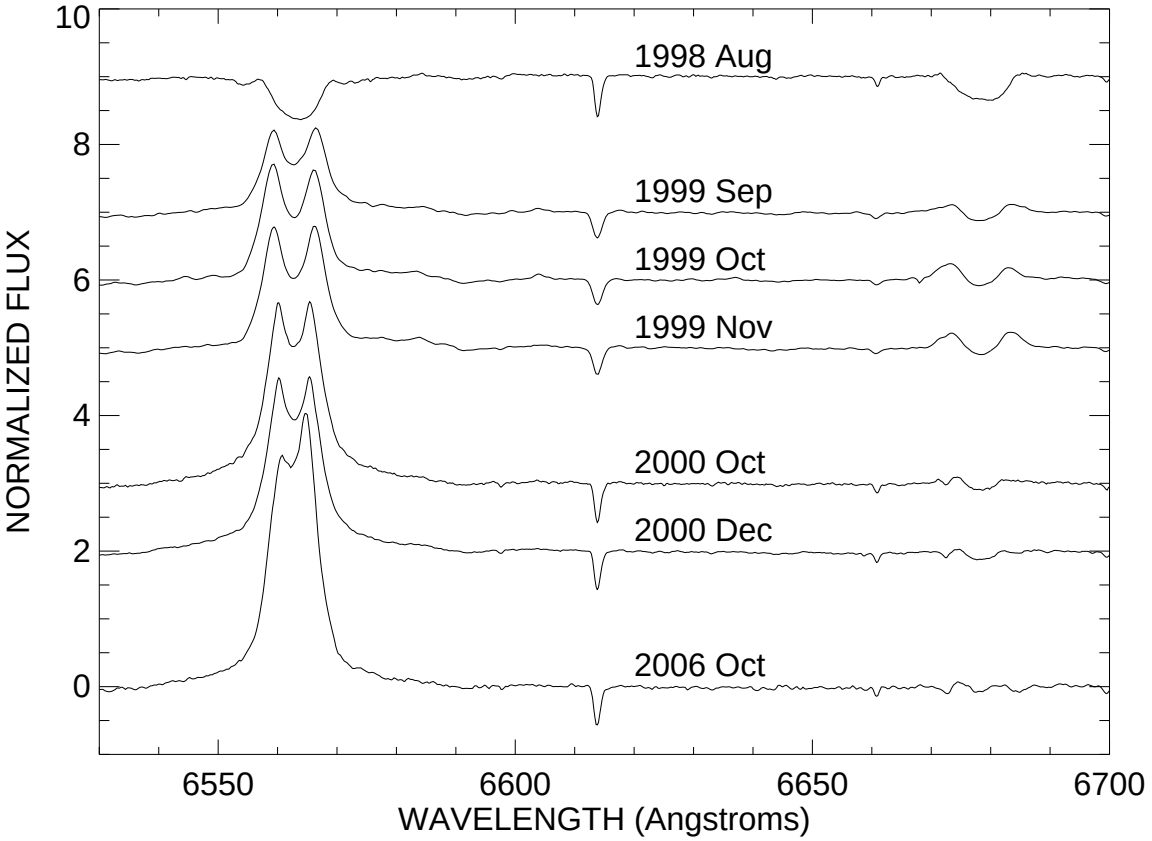

Fig. 2.— The average spectra of HDE 245770 from each of the runs plotted with their continua offset for clarity. Spectral intensity is scaled so that 100% of the continuum equals four units of normalized flux.

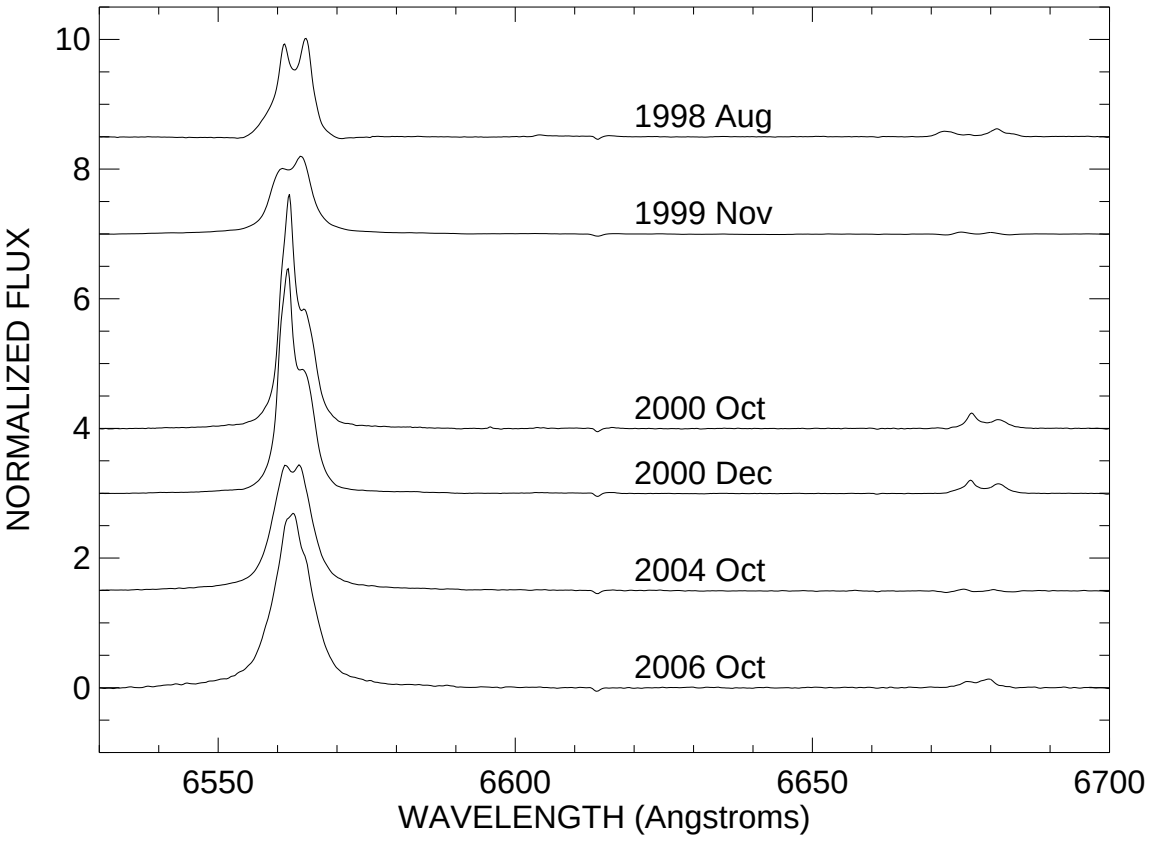

Fig. 3.— The mean spectra of X Per from each run (separated in rectified intensity for clarity). Spectral intensity is scaled so that 100% of the continuum equals one unit of normalized flux.

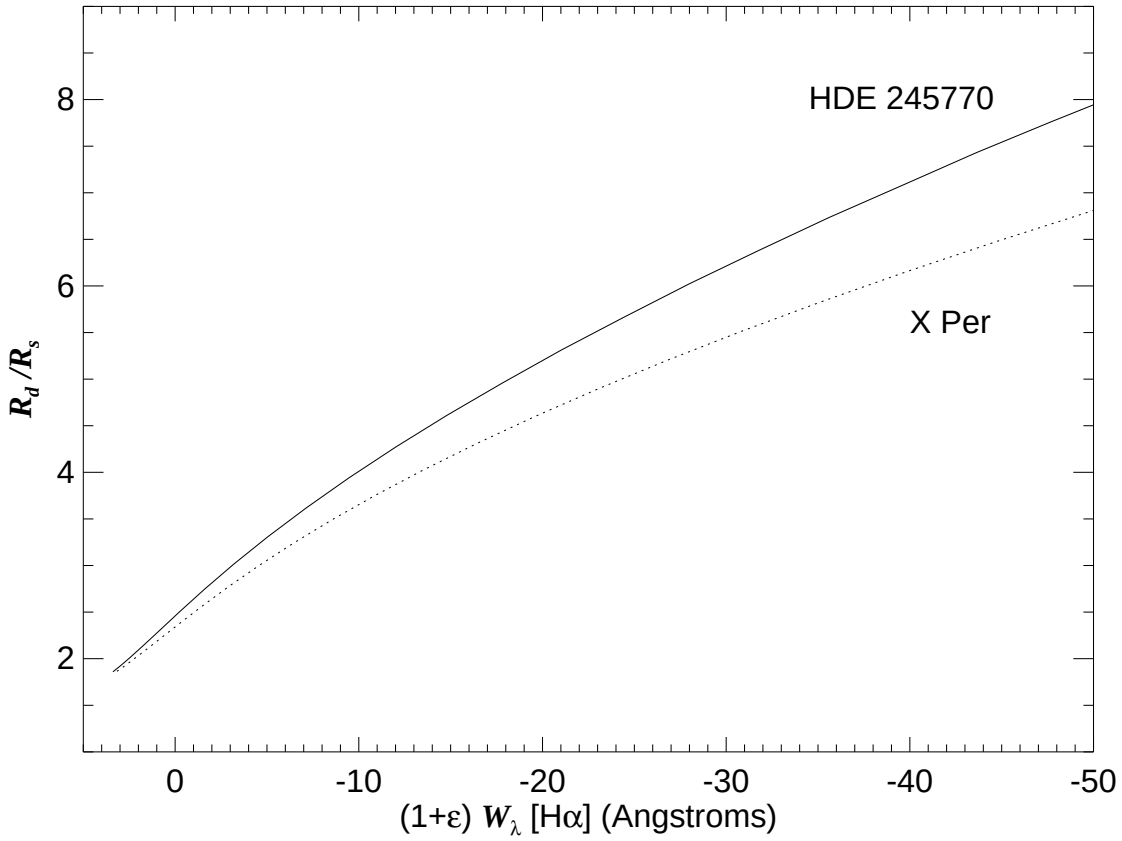

Fig. 4.— The model relation between rescaled Hα emission equivalent width and the ratio of disk radius (defined as the half maximum intensity radius of the integrated Hα flux) to the stellar radius.

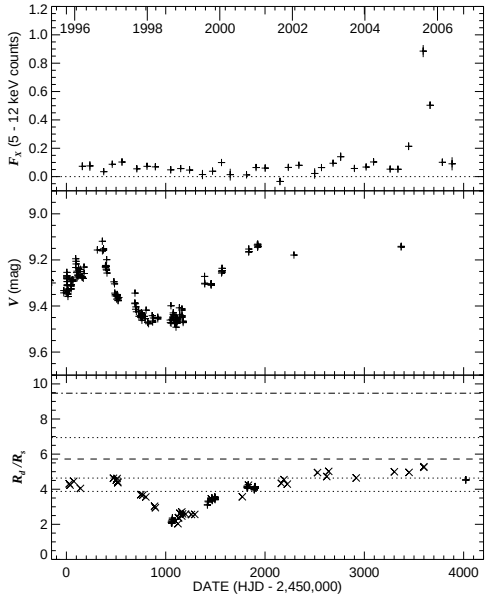

Fig. 5.— The time evolution of the X-ray flux (*top*), V (or J proxy) magnitude (*middle*), and disk radius (*bottom*) of HDE 245770. The disk radii are derived from the Hα equivalent widths and estimated V magnitudes (*plus signs* for data from Table 1 and *crosses* for values from earlier work). The dotted lines indicate disk radii associated with the historic mean levels of emission identified by Lyuty & Zaitseva (2000). The dashed line indicates the disk truncation radius for $n = 5$, and the dot-dashed line at the top marks a radius equal to the periastron separation.

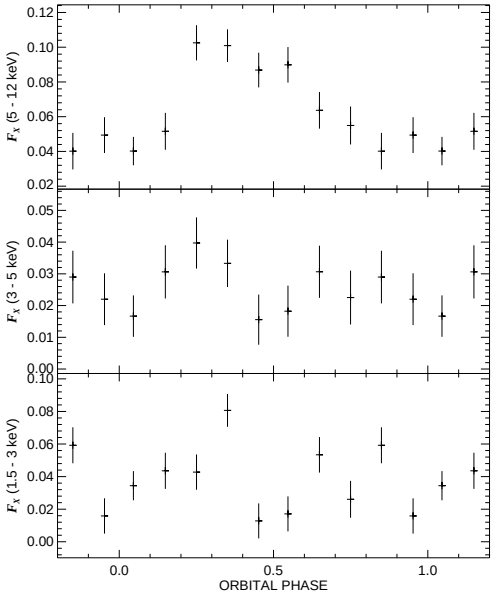

Fig. 6.— X-ray light curves of HDE 245770 from *RXTE*/ASM observations during quiescent dates formed by binning with the orbital ephemeris from Finger et al. (1994). The high energy band (*top panel*) appears to attain a maximum at a phase 0.3 past periastron.

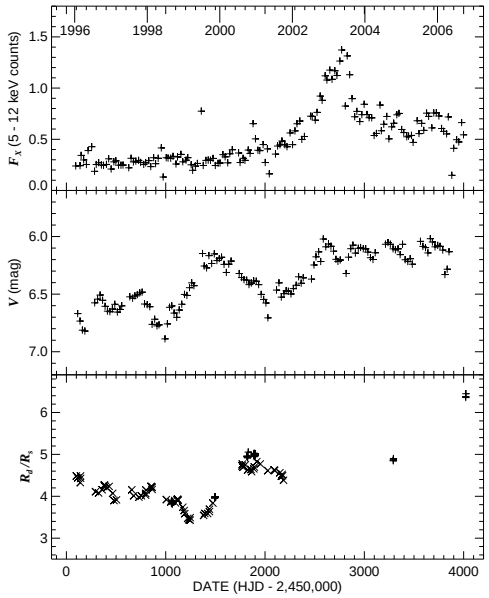

Fig. 7.— The time variations in X-ray flux (*top panel: RXTE*/ASM counts binned in 25 d increments), V magnitude (*middle panel:* AAVSO observations binned in 25 d increments), and the ratio of disk to stellar radius (*lower panel:* based upon the rescaled Hα equivalent width). The plus symbols in the lower plot indicate radii derived from our equivalent width measurements, while the crosses are other published measurements.

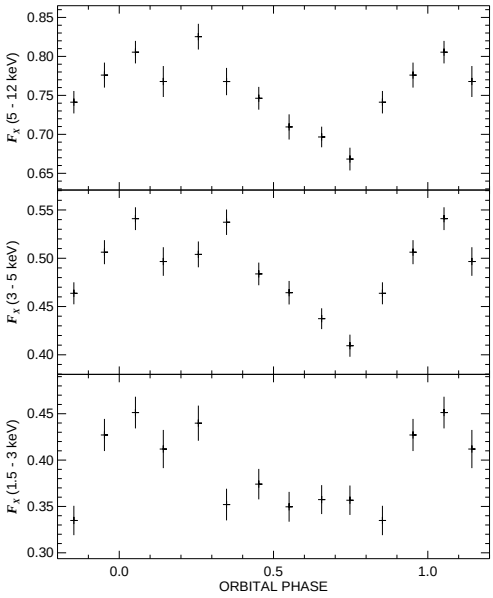

Fig. 8.— X-ray light curves of X Per from *RXTE*/ASM observations during active dates formed by binning with the orbital ephemeris from Delgado-Martí et al. (2001). The high energy band (*top panel*) appears to attain a maximum at a phase ≈ 0.25 past periastron. The vertical segments indicate the $\pm 1\sigma$ standard deviation of the mean within each bin.

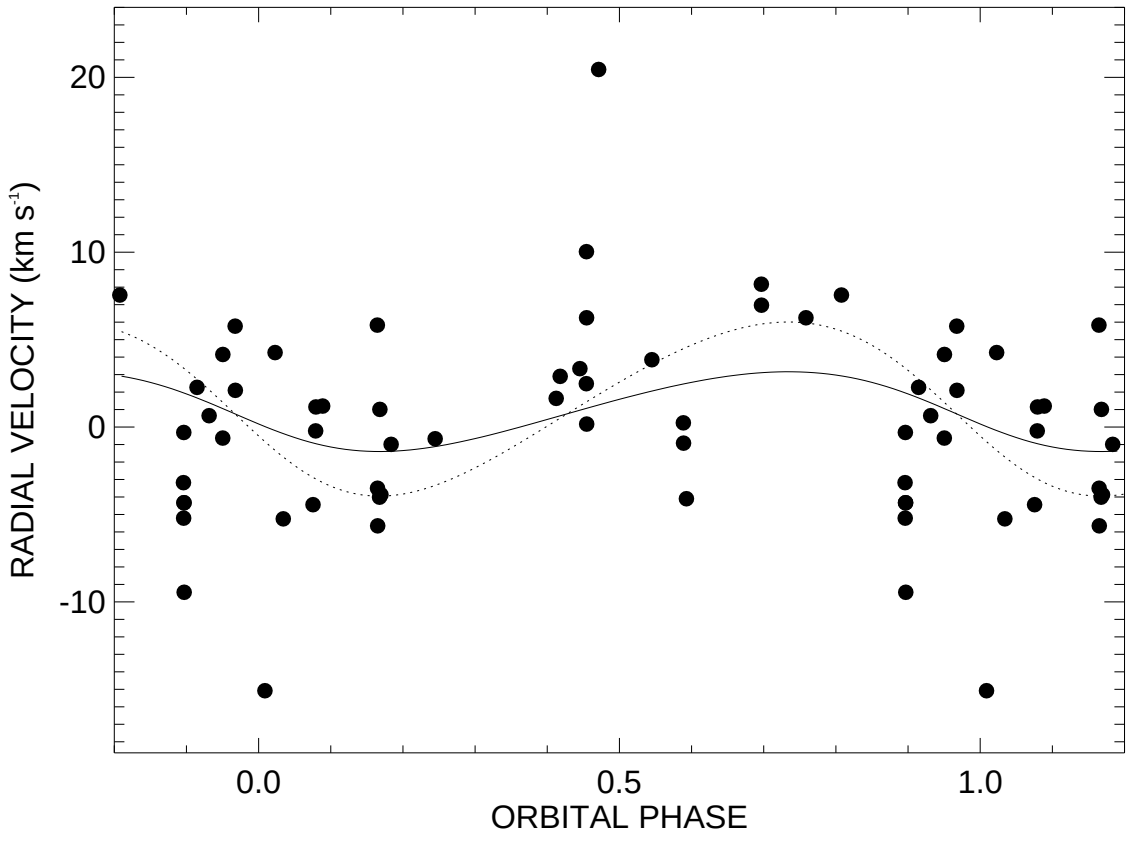

Fig. 9.— Radial velocities of X Per from *IUE* spectroscopy plotted against the orbital ephemeris of the X-ray pulsar. The solid line shows the nominal best fit of the Be star systemic velocity and semiamplitude (with all other parameters set by the pulsar orbit) while the dotted line shows a fit with the semiamplitude fixed at the 2σ upper limit.

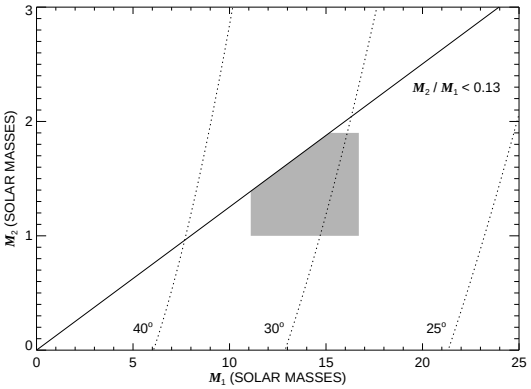

Fig. 10.— A mass plane diagram for X Per showing constraints on the Be star mass M_1 and the neutron star mass M_2. The solid line shows the upper limit on mass ratio determined from the *IUE* radial velocities, and the dotted lines show the mass relations for three values of orbital inclination. The shaded region shows the most probable range in masses for both components.